Available online at www.sciencedirect.com
ScienceDirect
Journal of Solid State Chemistry 180 (2007) 858–865
JOURNAL OF SOLID STATE CHEMISTRY
www.elsevier.com/locate/jssc

Structured diffuse scattering and polar nano-regions in the $Ba(Ti_{1-x}Sn_x)O_3$ relaxor ferroelectric system

Yun Liu[a], Ray L. Withers[a,*], Xiaoyong Wei[b], John D. Fitz Gerald[c]

[a]*Research School of Chemistry, Australian National University, Canberra, ACT 0200, Australia*
[b]*Electronic Materials Research Laboratory (EMRL), Xi'an Jiaotong University, Xi'an, China*
[c]*Research School of Earth Sciences, Australian National University, Canberra, ACT 0200, Australia*

Received 23 October 2006; accepted 5 December 2006
Available online 21 December 2006

Abstract

The observation via electron diffraction of relatively sharp $\mathbf{G}\pm\{001\}^*$ sheets of diffuse intensity arising from the large amplitude excitation of inherently polar, transverse optical modes of distortion in $Ba(Ti_{1-x}Sn_x)O_3$ (BTS), $0.1\leqslant x\leqslant 0.5$, samples, both at room temperature as well as liquid nitrogen temperature, shows that the polar nano-regions (PNRs) in these relaxor ferroelectric materials correspond to the same highly anisotropic $\langle 001\rangle$ chain dipoles as are characteristic of the normal ferroelectric end member $BaTiO_3$ itself. The correlation length along the chain of these 1-d PNRs can, in principle, be determined from the width of the observed $\{001\}^*$ diffuse sheets in reciprocal space and is estimated to be at least 5 nm even for the higher x samples. The distribution of the substitutional Sn ions thus appears to have only a minor effect upon the correlation length along the $\langle 001\rangle$ chain dipole directions. It is suggested that the role of the dopant Sn ions is not to directly induce PNRs but rather to set up random local strain fields preventing the condensation of long wavelength homogeneous strain distortions of the unit cell thereby suppressing transverse correlations of the $\langle 001\rangle$ chain dipoles and the development of long-range ordered ferroelectric state/s.

Keywords: Structured diffuse scattering; Electron diffraction; Polar nano-regions; Relaxor ferroelectrics; Extinction conditions; Strain

1. Introduction

Compositionally disordered relaxor ferroelectric, RFE, systems with their significantly broadened (relative to that of normal ferroelectric, NFE, materials) but still high magnitude peaks in dielectric permittivity as a function of temperature, have been of intense and continuing interest [1–14] ever since the pioneering work of Smolenskii [5]. This is both because of an intense interest in the physical mechanism underlying the so-called "diffuse phase transitions" (DPTs) characteristic of such RFEs (see e.g. Fig. 1) but most directly because of their huge range of applications (as electrostrictive and/or piezoelectric actuators and sensors [8,10,14], as electro-optic, elasto-optic and photorefractive elements [14], as high permittivity, tuneable dielectrics [10,15], etc.).

The $Ba(Ti_{1-x}Sn_x)O_3$ (BTS), $0\leqslant x\leqslant 0.5$, system is one of the earliest (see [5] and even earlier references contained therein) and most widely studied of such systems [8,16–25]. With increasing Sn content, the cubic paraelectric to tetragonal ferroelectric phase transition temperature (at T_c) characteristic of end member $BaTiO_3$ gradually decreases while the associated permittivity peak systematically broadens [18]. Simultaneously, the lower temperature tetragonal to orthorhombic, and orthorhombic to rhombohedral transition temperatures both increase until at $x=0.1$, the original three transition temperatures merge [18]. At and above this composition, the average structure unit cell remains metrically cubic and continuous at all temperatures, both above and below the remaining now significantly broadened peak in the dielectric permittivity [18] (at T_m).

While there is clear evidence for a macroscopic change in metric symmetry at T_c for $x<0.1$ there is no such evidence for any phase change at T_m in the case of the $x\geqslant 0.1$

*Corresponding author. Fax: +61 2 6125 0750.
E-mail address: withers@rsc.anu.edu.au (R.L. Withers).

0022-4596/$ - see front matter © 2006 Elsevier Inc. All rights reserved.
doi:10.1016/j.jssc.2006.12.013

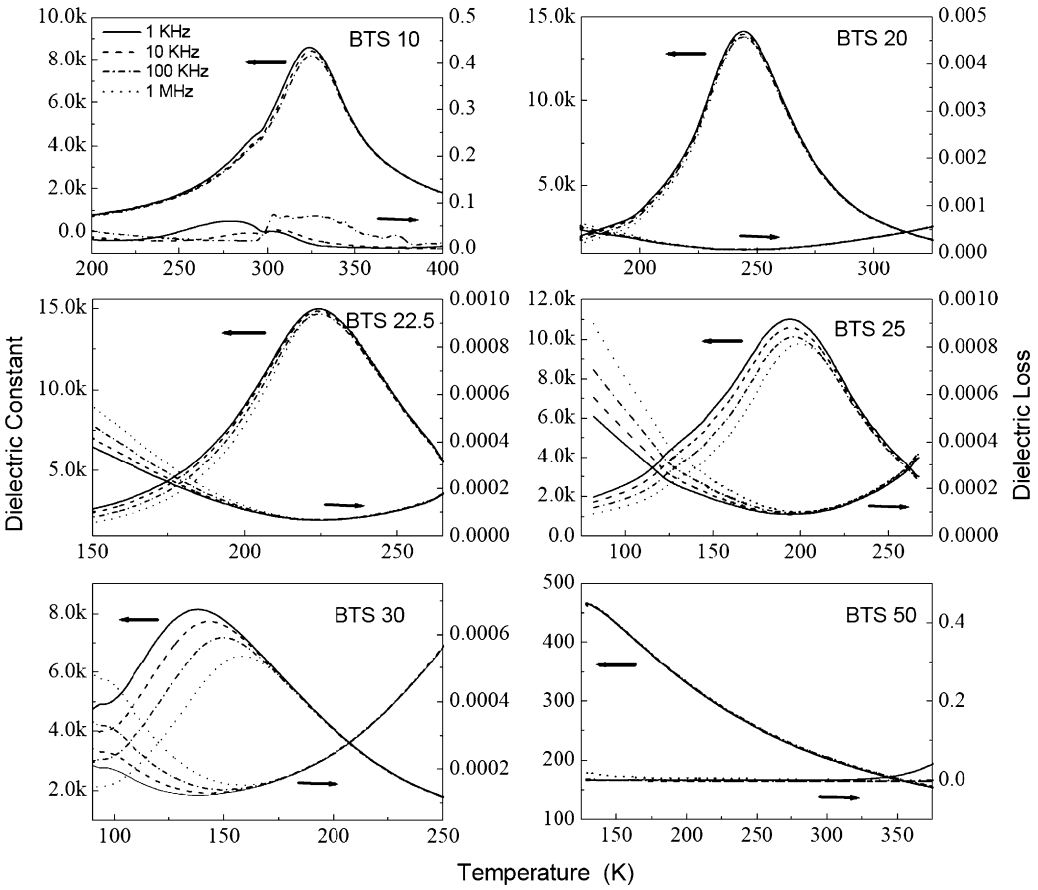

Fig. 1. The measured dielectric constant and dielectric loss versus temperature spectra at four separate frequencies (1, 10, 100 and 1 MHz) of the BTS10, 20, 22.5, 25, 30 and 50 samples.

samples. From the crystallographic point of view, there is thus a clear distinction between the $x<0.1$ and the $x\geqslant 0.1$ compositional regions. Within the latter metrically cubic BTS, $0.1\leqslant x\leqslant 0.5$, solid solution region, characteristic RFE behaviour [2,11,12] in the form of frequency-dependent T_m's only becomes clearly apparent [20,25] for $x>\sim 0.2$ (see e.g. Fig. 1). This has led various authors [18–20,25] to draw a distinction between so-called ferroelectrics exhibiting DPTs (for $x<\sim 0.2$) and "… true ferroelectric relaxors …" [9,25] (for $x>\sim 0.2$). The former are believed to undergo a DPT into a long-range ordered (presumably rhombohedral) ferroelectric state below T_m while the latter "… do not show long-range order when cooled in zero field to temperatures $T<T_m$ …" [25]. On the other hand, noticeable deviations from the Curie–Weiss law and significantly broadened peaks in the dielectric permittivity occur even for the lower x compositions [18,25]. Likewise, there is absolutely no evidence from the crystallographic point of view, including the new electron diffraction data presented in the current paper, for any phase change occurring as a function of composition from the $0.1\leqslant x<\sim 0.2$ samples to the $x>\sim 0.2$ samples.

The behaviour of NFEs such as $BaTiO_3$, at first glance, is quite different. It appears to be readily understandable in terms of the progressive softening of the frequency of a $\mathbf{q}=\mathbf{0}$, transverse optical (TO) phonon mode (involving off-centre $\langle 001\rangle$ displacements of the Ti and Ba ions in an opposite direction to the O ions) leading on lowering of temperature to a well-defined paraelectric to ferroelectric phase transition and to macro-sized FE domains below T_c [17]. By contrast, in the case of RFEs such as BTS, the mechanism underlying the observed behaviour is rather more difficult to understand. The qualitative differences in behaviour from NFEs are nowadays usually ascribed to the existence of polar nano-regions (PNRs) both above and below T_m in the case of RFEs. While there is near universal agreement as regards the existence and importance of PNRs in RFEs [1–25], the nature of such PNRs in BTS and their relationship (direct or indirect) to the Ti/Sn compositional disorder characteristic of BTS is still subject to considerable scientific debate.

Given the sensitivity of electron diffraction to weak features of reciprocal space difficult to detect by means of other diffraction techniques, the purpose of the current paper is to report the results of a detailed electron diffraction investigation of BTS searching for evidence of either PNRs and/or Ti/Sn ordering.

2. Experimental

2.1. Sample fabrication and lattice parameter determination

A series of $Ba(Ti_{1-x}Sn_x)O_3$, $x = 0.10$, 0.20, 0.225, 0.25, 0.30 and 0.50 (labelled BTS10, BTS20, BTS22.5, BTS25, BTS30, and BTS50 hereafter) powder samples were synthesized via conventional solid-state reaction using reagent-grade $BaCO_3$, $SrCO_3$, TiO_2 and SnO_2 as starting materials following the same synthesis procedure as described in [22]. The room temperature lattice parameters of the resultant single phase, metrically cubic samples were determined via powder X-ray diffraction using a Guinier–Hägg camera and Si powder as an internal standard. The lattice parameter of the samples was found to slowly but systematically increase as a function of composition from 4.0144 (8) Å for BTS10 to 4.0401 (3) Å for BTS50.

2.2. Electron diffraction

Electron diffraction at room temperature was carried out in a Philips EM 430 transmission electron microscope (TEM) operating at 300 kV on crushed grains of the powder sample dispersed onto holey carbon-coated copper grids. The typical diameter of the area from which the selected area electron diffraction patterns (EDPs) shown in Figs. 2 and 3 below obtained was ~0.5 μm. A liquid nitrogen cold stage was used for the low-temperature experiments. The lattice imaging work was carried out on a Philips CM30 TEM operating at 300 kV, again on crushed grains of the powder sample dispersed onto holey carbon-coated copper grids.

2.3. Dielectric property measurements

Powder samples were ground, pelleted and then annealed at 1400 °C for 2 h. The pellets were then polished on both sides. The resultant pellets had a diameter of 10 mm with a thickness of 0.3 mm. Their relative density was typically >95% while the average grain size was ~5–10 μm. They were then coated with silver paste for dielectric measurement using a high precision LCR meter (HP4284A) and an environmental box over a temperature range from liquid nitrogen to 250 °C. To prevent electrical breakdown along the edge of the pellets, only one side of the pellets were fully coated with silver paste. The remaining side of the pellets was also coated with silver paste, but only partially (to a diameter of 6 mm).

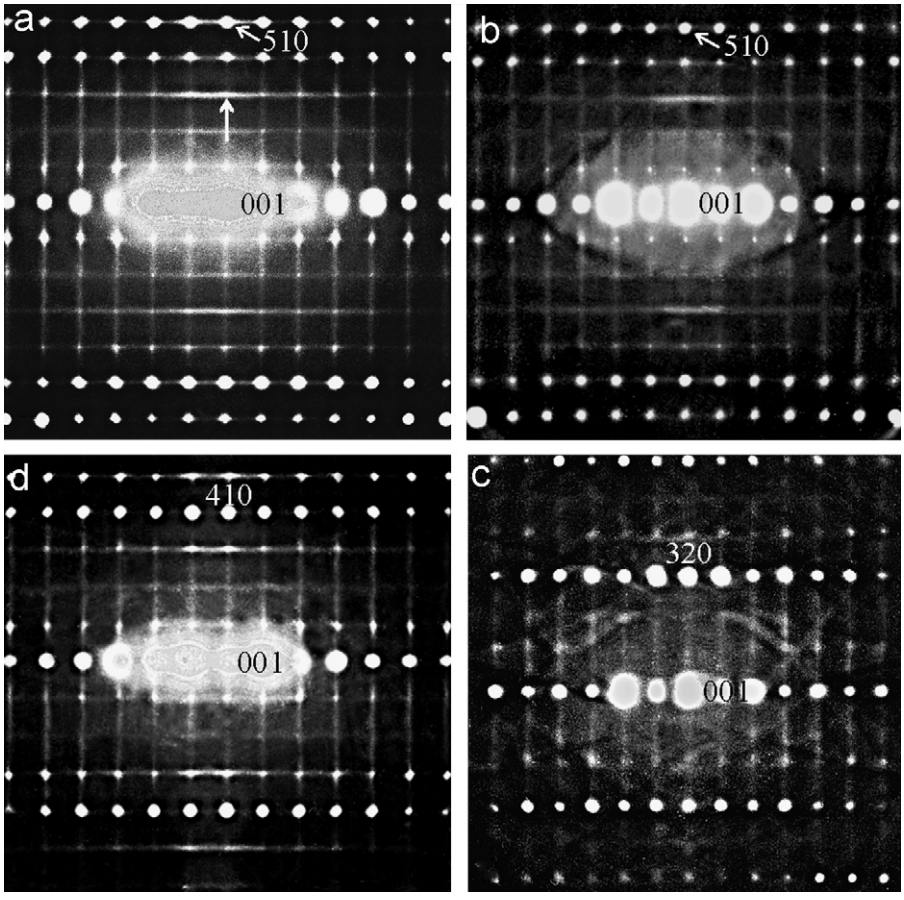

Fig. 2. ⟨−1,5,0⟩ zone axis EDPs of BTS10 at room temperature (a) and at liquid nitrogen temperature (b). (c) shows a typical ⟨−1,4,0⟩ zone axis EDP of BTS30 and (d) a typical ⟨−2,3,0⟩ zone axis EDP of BTS50.

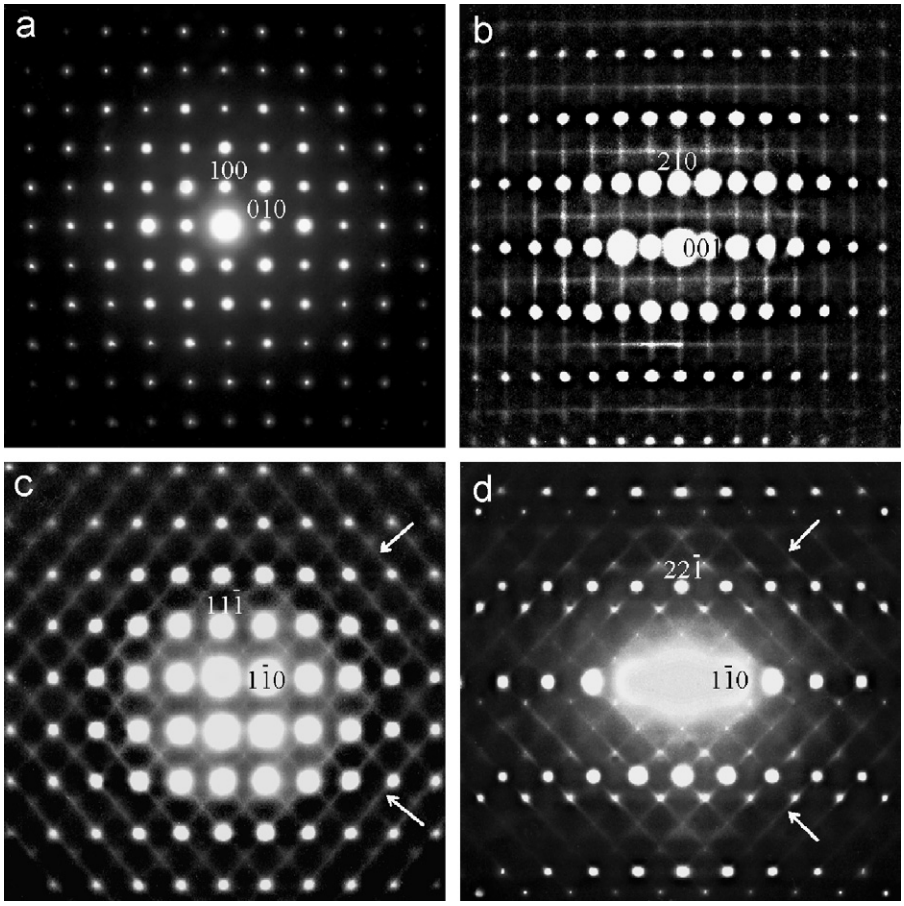

Fig. 3. Room temperature $\langle 001 \rangle$, $\langle -1,2,0 \rangle$, $\langle 112 \rangle$ and (d) $\langle 114 \rangle$ zone axis EDPs of (a) BTS30 and (b)–(d) BTS10 typical of the BTS, $0.1 \leqslant x \leqslant 0.5$, solid solution.

3. Results and discussion

The first thing to say is that very similar structured diffuse scattering, in the form of transverse polarized [26], quite sharp, {001}* sheets of diffuse intensity (to zeroth order), was observed right across the BTS, $x \geqslant 0.1$, solid solution, both at room temperature as well as at low (liquid nitrogen) temperature (see Figs. 2 and 3). The second important thing to say is that these {001}* sheets of diffuse intensity can be shown to arise from individual inherently polar, TO, displacive modes of distortion (see below) giving rise to what are, in effect, 1-d PNRs. It should be noted that, from the diffraction point of view, these polar displacive modes of distortion could be either static or dynamic in nature.

Despite the difference in dielectric behaviour as a function of composition (see Fig. 1), there is absolutely no evidence from the electron diffraction point of view of any change in behaviour occurring from the $0.1 \leqslant x < \sim 0.2$ samples to the $x > \sim 0.2$ samples and certainly no evidence that the former undergo a DPT into a long-range ordered ferroelectric state below T_m. Fig. 2a and b, for example, show essentially identical $\langle -1,5,0 \rangle$ zone axis EDPs of BTS10 at room temperature (a) and at liquid nitrogen temperature (b), while Fig. 2c shows a typical $\langle -1,4,0 \rangle$ zone axis EDP of BTS30 and Fig. 2d a typical $\langle -2,3,0 \rangle$ zone axis EDP of BTS50. Intriguingly, at the exact $\langle 010 \rangle$ zone axis orientation (see Fig. 3a), the diffuse streaking perpendicular to $\langle 001 \rangle$* seen at all other $\langle uv0 \rangle$ and $\langle uuw \rangle$ orientations (see Fig. 2 and 3b–d) disappears. This characteristic structured diffuse scattering, although weak, is nonetheless quite reproducible provided the crystal thickness and exposure time are sufficient to record it. Note that it is merely the visibility and not the width of the observed diffuse streaking that is dependent upon crystal thickness and exposure time.

In each case, note the presence of characteristic $\mathbf{G} \pm \langle hk0 \rangle$* diffuse streaking perpendicular to the three $\langle 001 \rangle$ real space directions running through the *Pm*–3*m* average structure Bragg reflections **G**. (The diffuse streaking running along the $\mathbf{G} \pm \gamma \langle 001 \rangle$*, γ continuous, direction of reciprocal space in Fig. 2 and 3b falls into a symmetry-related category to that just described e.g. the $\frac{3}{5} \langle 510 \rangle^* + \gamma \langle 001 \rangle^*$, γ continuous, diffuse streaking arrowed in Fig. 2a, $\equiv \langle 300 \rangle^* + \frac{3}{5} \langle 010 \rangle^* + \gamma \langle 001 \rangle^* = \mathbf{G} \pm \langle 0kl \rangle^*$ perpendicular to $\langle 100 \rangle$, etc.). Similar such EDPs were obtained from numerous different grains and are thus quite representative of the particular BTS composition.

The zero magnitude component of the individual $\mathbf{q} = \langle hk0 \rangle^*$, *h*, *k* continuous, modulation wave-vectors

(constituting the {001}* sheets of diffuse intensity) along the orthogonal ⟨001⟩ real space directions regardless of composition, i.e. regardless of the Ti/Sn composition ratio, is very significant. It rules out the possibility of Ti/Sn compositional ordering being responsible for the observed diffuse distribution. Consider the instructive counter-example of the $Nb_{1-x}{}^{V}Nb_{x}{}^{IV}O_{2-x}F_{1+x}$, $0 \leqslant x \leqslant 0.48$, solid solution where similar {001}* sheets of diffuse intensity implying 1-D correlated columns of atoms also occurs [27]. Here, however, the underlying origin of the observed diffuse distribution is compositional ordering, in this case 1-D O/F ordering along the ⟨001⟩ directions of the ReO_3-type average structure. The fixed component, ε, of the individual $\mathbf{q} = \langle hk\varepsilon \rangle^*$, h, k continuous, modulation wave-vectors constituting the {001}* sheets of diffuse intensity in this case is given by $\varepsilon = \frac{1}{3}[1+x]$, i.e. by the F/(O + F) ratio, and hence changes continuously with composition x [27]. In the case of BTS, however, $\varepsilon = 0$ and is completely independent of the Ti/Sn ratio. This strongly suggests that the observed diffuse distribution in the case of BTS has nothing directly to do with compositional Ti/Sn ordering.

Note that there is no diffuse intensity in the (100)* and (010)* reciprocal lattice planes passing through the origin i.e. there is no diffuse streaking along the $\mathbf{0} \pm \gamma[001]^*$ direction of reciprocal space in Fig. 2. (The apparent presence of diffuse streaking in the (001)* reciprocal lattice plane running through the origin in Fig. 2, e.g. along the [510]* direction of reciprocal space in Fig. 2a, can be attributed to multiple scattering associated with the strongly excited [001]* systematic row of Bragg reflections). Such an extinction condition arises from the transverse polarized nature of the individual displacive modes of distortion responsible for the observed diffuse distribution i.e. from the fact that $\mathbf{e}_\mu(\mathbf{q})$, the complex displacement eigenvector associated with each modulation wave-vector $\mathbf{q}$, must be transverse polarized or perpendicular to the direction of $\mathbf{q}$ itself for each atom μ in the average structure unit cell [26]. It necessitates an overwhelmingly dominant, transverse polarized, displacive origin for the intensity of the observed diffuse distribution [26,27].

The transverse polarized [26] nature of the diffuse distribution (i.e. the fact that its intensity is always strongest when looking out along directions of reciprocal space perpendicular to the direction of the streaking and goes to zero when looking along the direction of the streaking itself) gives rise to a strong azimuthal intensity variation of the observed $\mathbf{G} \pm \langle hk0 \rangle^*$ diffuse streaking. This is most apparent towards the edges of the EDPs shown in Figs. 2 and 3 where the effects of multiple scattering are much reduced cf., for example, the relative intensities of the $\mathbf{G} \pm \gamma[2,0,-1]^*$ and $\mathbf{G} \pm \gamma[0,2,-1]^*$ diffuse streaking at the arrowed positions of reciprocal space in Fig. 3c or those of the $\mathbf{G} \pm \gamma[4,0,-1]^*$ and $\mathbf{G} \pm \gamma[0,4,-1]^*$ diffuse streaking at the arrowed positions of reciprocal space in Fig. 3d.

In this case, where the observed diffuse distribution takes the form of {001}* sheets of diffuse intensity perpendicular to each of the three ⟨001⟩ directions of the underlying *Pm*–3*m* average structure, this implies that the atomic displacements responsible for the observed {001}* sheets of diffuse intensity must be polarized along the ⟨001⟩ directions themselves i.e. $\mathbf{e}_\mu(\mathbf{q} = \langle hk0 \rangle^*) = e_\mu \langle 001 \rangle$ for each independent atom. While these displacements must be correlated from unit cell to unit cell along the ⟨001⟩ column direction (with an correlation length estimated from the width of the observed diffuse streaking of at least 5 nm, even for the higher x compositions), the observed {001}* sheets of diffuse intensity imply that there is very little if any correlation in the transverse direction from any one such ⟨001⟩ column to the next. In conjunction with the zero magnitude component of the individual $\mathbf{q} = \langle hk0 \rangle^*$ modulation wave-vectors, the above observations rule out the possibility of Ti/Sn compositional ordering playing any direct role in the observed diffuse distribution [26].

That such correlated off-centre ⟨001⟩ displacements give rise to what are, in effect, 1-d PNRs as stated above requires proof that the individual transverse polarized $\mathbf{q} = \langle hk0 \rangle^*$ modes of distortion observed are inherently polar i.e. TO in nature rather than simply transverse acoustic. The simplest way to show this is to consider the characteristic intensity distribution within the observed $\mathbf{G} \pm \{001\}^*$ sheets of diffuse intensity (being careful to take into account the sometimes distorting effect of multiple scattering where it is apparent—see e.g. Fig. 4 of [26]). Consider, for example, the relative intensities of the $\frac{h}{4}\langle 410 \rangle^* + \gamma \langle 001 \rangle^*$ diffuse streaking apparent in Fig. 2c. It is clear that the $h = 1$, 3 and 5 streaks of this form are considerably more intense than the $h = 2$ and 4 streaks, indeed the latter appears to be virtually systematically absent. Likewise, the h odd streaks of the $\frac{h}{2}\langle 210 \rangle^* + \gamma \langle 001 \rangle^*$ diffuse streaking apparent in Fig. 3b are quite strong whereas the h even streaks of this form are to all intents and purposes again systematically absent.

'Extinction conditions' of the latter type, even when only approximate, are invaluable. Indeed, in the current case, they can be used to 'solve for' the real space origin of the observed diffuse distribution [26,28,29]. Writing the displacement of the μth atom in the unit cell $\mathbf{t}$ away from its average structure position at $(\mathbf{r}_\mu + \mathbf{t})$ in the form:

$$\begin{aligned}\mathbf{u}_\mu(\mathbf{r}_\mu + \mathbf{t}) &= \sum\nolimits_{\mathbf{q}} \mathbf{e}_\mu(\mathbf{q}) \exp\, 2\pi i \mathbf{q}(\mathbf{r}_\mu + \mathbf{t}), \\ &= \sum\nolimits_{q} (Re\{\mathbf{e}_\mu(\mathbf{q})\} \cos 2\pi \mathbf{q}(\mathbf{r}_\mu + \mathbf{t}), \\ &\quad - Im\{\mathbf{e}_\mu(\mathbf{q})\} \sin\, 2\pi \mathbf{q}(\mathbf{r}_\mu + \mathbf{t})) \ldots \end{aligned} \quad (1)$$

and making the assumption that the diffuse intensity observed at $\mathbf{G} \pm \mathbf{q}$ ($\mathbf{G}$ an average structure reciprocal lattice vector) arises solely from displacive modulation waves associated with the modulation wave-vector $\mathbf{q}$, then the structure factor $F(\mathbf{G} + \mathbf{q})$ can be shown to be proportional to

$$F(\mathbf{G} + \mathbf{q}) \alpha \Sigma_\mu f_\mu \, exp[-2\pi i \mathbf{G} \bullet \mathbf{r}_\mu] \times (2\pi[\mathbf{G} + \mathbf{q}]\mathbf{e}_\mu(\mathbf{q})) \ldots \quad (2)$$

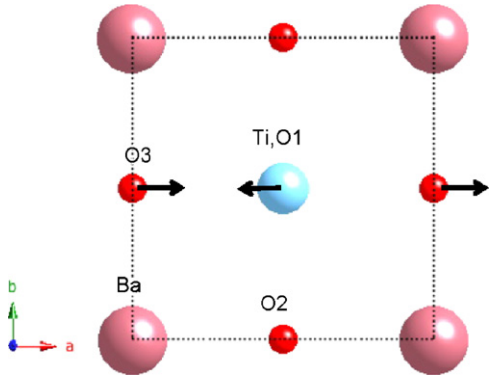

Fig. 4. Shows the five distinct ions per parent perovskite unit cell of BTS: Ba at 0,0,0; $Ti_{1-x}Sn_x$ at $\frac{1}{2},\frac{1}{2},\frac{1}{2}$; O1 at $\frac{1}{2},\frac{1}{2},0$; O2 at $\frac{1}{2},0,\frac{1}{2}$ and O3 at $0,\frac{1}{2},\frac{1}{2}$ along with the relevant inherently polar displacive shifts along $\langle 100\rangle$ deduced from extinction conditions associated with the observed diffuse distribution.

(see [26] for more details). In the current case of BTS, there are five distinct atoms per parent unit cell: Ba at $0,0,0$; $Ti_{1-x}Sn_x$ at $\frac{1}{2},\frac{1}{2},\frac{1}{2}$; O1 at $\frac{1}{2},\frac{1}{2},0$; O2 at $\frac{1}{2},0,\frac{1}{2}$ and O3 at $0,\frac{1}{2},\frac{1}{2}$ (see Fig. 4) for each of which we need to know $\mathbf{e}_\mu$. It has already been shown above that $\mathbf{e}_\mu(\mathbf{q}=\langle hk0\rangle^*)=\mathrm{e}_\mu\langle 001\rangle$ for each of these five independent ions. In the case of the $\frac{h}{2}\langle 210\rangle^*+\gamma\langle 001\rangle^*=h\mathbf{a}^*+\langle 0,\frac{h}{2},\gamma\rangle^*$ diffuse streaking apparent in Fig. 3b, where $\mathbf{q}$ takes the form $\langle 0,\frac{h}{2},\gamma\rangle^*$ perpendicular to $\langle 100\rangle$, this amounts to the condition $\mathbf{e}_\mu(\mathbf{q}=\langle 0kl\rangle^*)=\mathrm{e}_\mu\langle 100\rangle$ for each of these five independent ions.

Under the obviously fairly good assumption that $F(\mathbf{G}+\mathbf{q})=0$ at $(\mathbf{G}+\mathbf{q})=[2,1,0+\gamma]^*$, $[2,1,1+\gamma]^*$, $[4,2,0+\gamma]^*$ and $[4,2,1+\gamma]^*$, substitution into Eq. (2) above then requires that $\mathrm{e}_{Ba}=\mathrm{e}_{O1}=\mathrm{e}_{O2}=0$ while $f_{Ti,Sn}\mathrm{e}_{Ti}+f_O\mathrm{e}_{O3}=0$. Note that O3 and Ti necessarily move in opposite directions. Given that $f_{Ti}/f_O=2.27$ at $g_{210}=0.555\,\text{Å}^{-1}$ and 2.29 at $g_{420}=1.110\,\text{Å}^{-1}$ [30], the above equality implies that $e_{O3}\sim-2.28e_{Ti}$ (see Fig. 4). The strength of the h odd streaks of the $\frac{h}{2}\langle 210\rangle^*+\gamma\langle 001\rangle^*$ diffuse streaking apparent in Fig. 3b is entirely consistent with the above values in that the sign of the O3 contribution to the overall structure factor relative to that of the $Ti_{1-x}Sn_x$ ions is reversed by the fact that h is odd leading to the observed large intensity. Likewise, the strength of the h odd, $\frac{h}{2}\langle 410\rangle^*+\gamma\langle 001\rangle^*$ diffuse streaking in Fig. 2c relative to the h even diffuse streaking is also quite consistent with the relative magnitudes of the above determined displacement eigenvectors. The fact that the oxygen ions necessarily move in the opposite sense to the Ti ions confirms the inherently dipolar nature of the TO modes of distortion responsible for the observed diffuse distribution (see Fig. 4), as stated above.

From the diffraction point of view, it is of course not possible to distinguish between static and dynamic disorder so that it is not possible to say whether these inherently 1-d PNRs or dipole moments are static or dynamic. Whether static or dynamic, however, the diffraction evidence clearly demonstrates extremely anistropic, anti-correlated behaviour of the off-centre displacements of the Ti and O ions ultimately responsible for the observed dielectric behaviour of BTS. Clearly, the development of long-range ferroelectric behaviour requires not just the slowing down and freezing-in of these 1-d PNRs at T_m but, most importantly, their transverse correlation from one such $\langle 001\rangle$ chain to the next.

At this stage, the next important thing to say is that a virtually identical diffuse intensity distribution has long been known to be characteristic of the high temperature, paraelectric phase (for several hundred degrees above T_c) of NFEs such as $BaTiO_3$ itself and $KNbO_3$ [31–33]. Indeed very similar diffuse scattering also occurs in the tetragonal ferroelectric phase of $BaTiO_3$ as can be seen from a comparison of Fig. 7 of [34] with Fig. 2a). A similar diffuse distribution has recently also been shown to be characteristic of $CaCu_3Ti_4O_{12}$ [35]. This suggests that the existence of such highly anisotropic 1-d PNRs (whether static or dynamic) is not dependent upon compositional disorder but rather seems to be characteristic of perovskite-related structures containing a significant number of corner-connected TiO_6 octahedral units with tolerance factors >1. (It is, however, important to note that the absence of characteristic RFE behaviour such as that shown in Fig. 1 in the case of $BaTiO_3$ itself shows that the mere existence of such 1-d PNRs is not sufficient in and of itself to cause RFE behaviour). Along any one such $\langle 001\rangle$ chain dipole, Ti and O ions are shifted off-centre (in the opposite sense) in a correlated fashion along the same $\langle 001\rangle$ direction giving rise to a large linear dipole along the particular $\langle 001\rangle$ direction, as originally proposed by Comés et al. [31, 33] and Lambert and Comes [32] in the case of $BaTiO_3$ itself. $\{001\}^*$ sheets of diffuse intensity arise because of the lack of transverse correlation from one such chain dipole to the next.

There has, of course, been much controversy in the literature on $BaTiO_3$ as to whether these linear chain dipoles required by the diffraction evidence are static or dynamic in character [31–34,36–39]. As discussed above, however, whether static or dynamic, it is clear that the development of long-range ferroelectric order depends critically not just on the presence of (static) 1-d PNRs but, equally importantly, on their transverse correlation from one $\langle 001\rangle$ chain to the next. Returning to BTS, note that the narrowness of the observed $\{001\}^*$ sheets of diffuse intensity even at relatively high x (see e.g. Fig. 2c for $x=0.3$, where three in every 10 Ti ions along any one $\langle 001\rangle$ string direction are on average replaced by Sn ions) implies that the correlated polar shifts along the $\langle 001\rangle$ direction are significantly longer than the average Sn–Sn separation distance. Even in the case of $x=0.5$, where the observed diffuse scattering is clearly significantly weaker the intra-chain correlation length still appears to be quite long (see Fig. 2d).

Absolutely no evidence could be found for Ti/Sn ordering at any composition or temperature within the BTS, $0.1\leqslant x\leqslant 0.5$, solid solution. As discussed above, it is not possible to interpret the observed $\mathbf{G}\pm\{001\}^*$ diffuse

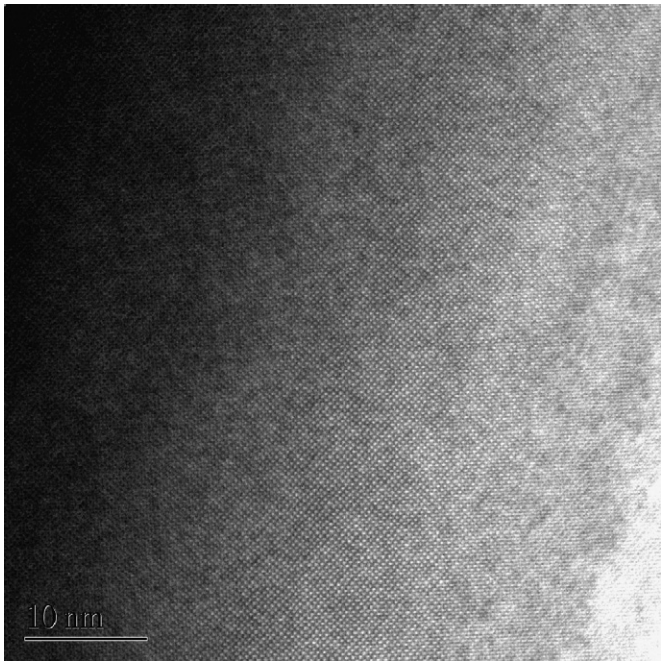

Fig. 5. A typical ⟨001⟩ HREM lattice image of BTS 30. No evidence has been found in any such lattice images for a domain structure of any sort or evidence for Ti/Sn ordering.

distribution in terms of Ti/Sn ordering and associated relaxation. In addition, no obvious evidence could be found in bright field (BF) or HREM lattice images (see e.g. the room temperature ⟨001⟩ HREM lattice image of BTS30 shown in Fig. 5) for a domain structure at any composition, in particular no such evidence could be found for the BTS10 sample.

Note that the continued presence of $\mathbf{G}\pm\{001\}^*$ diffuse intensity at liquid nitrogen temperatures is also incompatible with a low temperature rhombohedral ferroelectric phase. The DPTs apparent in these BTS samples (see Fig. 1), including the lower x compositions, are thus clearly not a result of a DPT into a long-range ordered ferroelectric state below T_m [25] but rather are a result of a dynamic freezing or glass-like transition [11,12] involving the slowing down of the dipolar dynamics of the 1-d PNRs implied by the existence of the structure diffuse distribution. Given the continued existence of the same structured diffuse distribution on either side of T_m, it is clear that none of the BTS, $0.1 \leqslant x \leqslant 0.5$, samples can show long-range ferroelectric order when cooled in zero field to temperatures $< T_m$ i.e. application of an external field is necessary to induce long-range ferroelectric order. This suggests that the primary role of the applied electric field below T_m is to induce transverse correlation from one such ⟨001⟩ chain to the next.

As is well known, the interstitial Ba ion in $BaTiO_3$ is significantly over-bonded while the Ti ions are significantly under-bonded in the ideal *Pm–3m* structure type. Given that the Sn^{4+}–O distance in an ideal octahedron should be ~2.055 Å whereas the ideal Ti^{4+}–O distance should be ~1.965 Å [40], it is not surprising that increasing substitution of Ti ions by Sn ions in the BTS solid solution leads to an increase in the cubic lattice parameter of the BTS samples. It might also be expected to set up a not inconsiderable local strain field. The surprising result of this paper is that these local strain fields do not appear to have a very strong effect upon the longitudinal correlation length of the 1-d PNRs or chain dipoles along the ⟨001⟩ direction (see Figs. 2 and 3). The only observable difference as x increases is that the structured diffuse scattering appears to become systematically weaker, particularly at $x = 0.5$. That the diffuse systematically weakens with increasing x is consistent both with the reduction in off-centre Ti ions, as well as with the measured systematic reduction in the room temperature dielectric constant, with increasing x of the BTS samples, as shown in Fig. 1. On the other hand, the optical study [17] of these BTS samples shows clearly that the Sn content has a very strong effect upon the size of the ferroelectric domains once induced by an applied electric field.

This suggests that the prime role of the dopant Sn ions is not to introduce the PNRs. As discussed above, they already exist in the non-chemically disordered end member $BaTiO_3$ itself. Rather the role of the dopant Sn ions appears to be to set up random local strain fields thereby suppressing homogeneous long wavelength strain distortion of the underlying cubic lattice, the transverse correlation of the pre-existing static 1-d PNRs (below T_m) and a transition into a long-range ordered ferroelectric state. It is interesting in this context to note the comments of successive authors in the case of $BaTiO_3$ to the effect that "… strain coupling is … crucial in producing the correct succession of low-symmetry (ferroelectric) phases …" [39,41,42]. It is not too difficult to envisage that local disorder associated with Sn doping might well suppress a homogeneous strain or lattice distortion below T_m and hence prevent the condensation of a long-range ordered ferroelectric state without the application of an applied electric field. This is consistent with the disappearance of the original three phase transitions in pure $BaTiO_3$ upon increasing the Sn dopant level to $x \geqslant 0.1$ [18].

Returning to the dielectric properties of BTS, Fig. 1 shows the measured dielectric constant and dielectric loss versus temperature spectra at four separate frequencies (1, 10, 100 and 1 MHz) of the BTS10, 20, 22.5, 25, 30 and 50 samples investigated by electron diffraction. Note the systematic lowering of T_m and the broadening of the peak in the dielectric constant at T_m with increasing Sn content. Clearly the thermal energy required to flip the sign of the dipole moments of the 1-d PNRs systematically reduces with increasing Sn content. Note further that T_m for BTS10 is around 325 K and does not appear to be frequency dependent. Likewise, T_m for BTS20 appears to be essentially frequency-independent. By BTS 22.5, however, characteristic frequency-dependent RFE behaviour is clearly apparent both in the dielectric constant and dielectric loss spectra. From the dielectric properties' point of view, there thus appears to be some sort of transition

around $x \sim 0.2$. From the diffraction point of view, however, as discussed above, there is absolutely nothing to distinguish the low x from the high x samples within the $Ba(Ti_{1-x}Sn_x)O_3$, $0.1 \leqslant x \leqslant 0.5$, solid solution.

4. Summary and conclusions

A highly structured characteristic diffuse intensity distribution in the form of transverse polarized, quite sharp, {001}* sheets of diffuse intensity arising from the large amplitude excitation of individual, inherently dipolar, TO modes of distortion, has been observed right across the BTS, $x \geqslant 0.1$, solid solution, both at room temperature as well as at low (liquid nitrogen) temperature. This diffuse distribution requires the existence of anti-correlated off-centre $\langle 001 \rangle$ displacements of Ti and O ions giving rise to what are, in effect, 1-d PNRs (whether static or dynamic). The similarity of the observed diffuse distribution both above and below T_m can only be understood in terms of a dynamic freezing or glass-like transition of the dipolar dynamics of these 1-d PNRs (see Fig. 4) on cooling below T_m. The observed RFE behaviour of BTS samples at high x is not associated with the existence of these 1-d PNRs but rather with the suppression of homogeneous strain distortion below T_m induced by the inhomogeneous distribution of the dopant Sn ions leading in turn to the suppression of transverse correlation of the pre-existing 1-d PNRs (below T_m).

References

[1] X. Yao, Z. Chen, L. Cross, J. Appl. Phys. 54 (1983) 3399–3403.
[2] L. Cross, Ferroelectrics 76 (1987) 241–267.
[3] V. Isupov, Ferroelectrics 90 (1989) 113–118.
[4] G. Burns, F. Dacol, Ferroelectrics 104 (1990) 25–35.
[5] G. Smolenskii, J. Phys. Soc. Japan 28 (1970) 26–37.
[6] N. Setter, L. Cross, J. Mater. Sci. 15 (1980) 2478–2482.
[7] D. Viehland, S. Jiang, L. Cross, J. Appl. Phys. 68 (1990) 2916–2921.
[8] J. Cieminski, H. Beige, J. Phys. D: Appl. Phys. 24 (1991) 1182–1186.
[9] L. Cross, Ferroelectrics 151 (1994) 305–320.
[10] K. Uchino, Ferroelectrics 151 (1994) 321–333.
[11] G. Samara, J. Phys.: Condens. Matter 15 (2003) R367–R411.
[12] A. Bokov, Z.-G. Ye, J. Mater. Sci. 41 (2006) 31–52.
[13] R. Blinc, Ferroelectrics 330 (2006) 1–7.
[14] W. Kleemann, J. Mater. Sci. 41 (2006) 129–136.
[15] S. Lu, Z. Xu, H. Chen, Appl. Phys. Lett. 85 (2004) 5319–5321.
[16] J. Lin, T. Wu, J. Appl. Phys. 68 (1990) 985–993.
[17] M. Oh, K. Uchino, L. Cross, J. Am. Ceram. Soc. 77 (1994) 2809–2816.
[18] N. Yasuda, H. Ohwa, S. Asano, Jpn. J. Appl. Phys. 35 (1996) 5099–5103.
[19] X. Wei, Y. Feng, X. Yao, Appl. Phys. Lett. 83 (2003) 2031–2033.
[20] X. Wei, Y. Feng, X. Wan, X. Yao, Ceram. Int. 30 (2004) 1397–1400.
[21] X. Wei, Y. Feng, L. Hang, X. Yao, Ceram. Int. 30 (2004) 1401–1404.
[22] X. Wei, Y. Feng, L. Hang, S. Xia, L. Jin, X. Yao, Mater. Sci. Eng. B 120 (2005) 64–67.
[23] L. Geske, H. Beige, H.-P. Abicht, V. Mueller, Ferroelectrics 314 (2005) 97–104.
[24] V. Mueller, A. Kouvatov, R. Steinhausen, H. Beige, H.-P. Abicht, Integr. Ferroelectr. 63 (2004) 81–84.
[25] V. Mueller, H. Beige, H.-P. Abicht, Appl. Phys. Lett. 84 (2004) 1341–1343.
[26] R.L. Withers, Z. Für Kristallogr. 220 (2005) 1027–1034.
[27] F.J. Brink, L. Norén, R.L. Withers, J. Solid State Chem. 155 (2004) 2177–2182.
[28] M.I. Aroyo, H. Boysen, J.M. Pérez-Mato, Appl. Phys. A (Suppl.) 74 (2002) 1043–1045.
[29] J.M. Pérez-Mato, M. Aroyo, J. Hlinka, M. Quilichini, R. Currat, Phys. Rev. Lett. 81 (1998) 2462–2465.
[30] A.J.C. Wilson (Ed.), International Tables for Crystallography, vol. C, Kluwer Academic, Dordrecht,, 1995 Table 4.3.1.1.
[31] R. Comés, M. Lambert, A. Guinier, Solid State Commun. 6 (1968) 715–719.
[32] M. Lambert, R. Comés, Solid State Commun. 7 (1969) 305–308.
[33] R. Comés, M. Lambert, A. Guinier, Acta Crystallogr. A 26 (1970) 244–254.
[34] J. Harada, G. Honjo, J. Phys. Soc. Japan 22 (1967) 45–57.
[35] Y. Liu, R.L. Withers, X.Y. Wei, Phys. Rev. B 72 (2005) 134104–134114.
[36] A. Hüller, Solid State Commun. 7 (1969) 589–591.
[37] K. Müller, W. Berlinger, Phys. Rev. B 34 (1986) 6130–6137.
[38] J.-M. Kiat, G. Baldinozzi, M. Dunlop, C. Malibert, B. Dkhil, C. Ménoret, O. Masson, M.-T. Fernandez-Diaz, J. Phys. Condens. Matter 12 (2000) 8411–8425.
[39] B. Zalar, V. Laguta, R. Blinc, Phys. Rev. Lett. 90 (2003) 037601–037614.
[40] N. Brese, M. O'Keeffe, Acta Crystallogr. B 47 (1991) 192–197.
[41] W. Zhong, D. Vanderbilt, K. Rabe, Phys. Rev. Lett. 73 (1994) 1861–1864.
[42] A. Chaves, F. Barreto, R. Nogueira, B. Zeks, Phys. Rev. B 13 (1976) 207–212.